



# 3D gut-liver chip with a PK model for prediction of first-pass metabolism

Dong Wook Lee<sup>1</sup> · Sang Keun Ha<sup>2</sup> · Inwook Choi<sup>2</sup> · Jong Hwan Sung<sup>1</sup>

Published online: 7 November 2017  
© Springer Science+Business Media, LLC 2017

**Abstract** Accurate prediction of first-pass metabolism is essential for improving the time and cost efficiency of drug development process. Here, we have developed a microfluidic gut-liver co-culture chip that aims to reproduce the first-pass metabolism of oral drugs. This chip consists of two separate layers for gut (Caco-2) and liver (HepG2) cell lines, where cells can be co-cultured in both 2D and 3D forms. Both cell lines were maintained well in the chip, verified by confocal microscopy and measurement of hepatic enzyme activity. We investigated the PK profile of paracetamol in the chip, and corresponding PK model was constructed, which was used to predict PK profiles for different chip design parameters. Simulation results implied that a larger absorption surface area and a higher metabolic capacity are required to reproduce the *in vivo* PK profile of paracetamol more accurately. Our study suggests the possibility of reproducing the human PK profile on a chip, contributing to accurate prediction of pharmacological effect of drugs.

**Keywords** Gut-liver chip · First-pass metabolism · PK model · Oral drugs

---

**Electronic supplementary material** The online version of this article (<https://doi.org/10.1007/s10544-017-0242-8>) contains supplementary material, which is available to authorized users.

✉ Jong Hwan Sung  
jhsung22@hongik.ac.kr; jhsung22@gmail.com

<sup>1</sup> Department of Chemical Engineering, Hongik University,  
Seoul 121-791, Korea  
<sup>2</sup> Korea Food Research Institute, Seongnam-si, Gyeonggi-do, Republic  
of Korea

## 1 Introduction

Orally administered drugs undergo a complex process of absorption, distribution, metabolism and elimination. In particular, they go through absorption in the gut, followed by metabolism in the liver before entering the systemic circulation, which is known as the first-pass metabolism. Many drug candidates fail due to unforeseen toxicity or lack of efficacy, which is largely affected by the first-pass metabolism (Carriere et al. 2001; Strovel et al. 2004; Kaitin 2010). Animal study carries not only ethical issues, but also the issue of animal to human extrapolation (Sankar 2005; Greek and Menache 2013).

*In vitro* models have the advantages of high-throughput experiment, but the lack of physiological relevance has been the main limiting factor. One of the reasons for inaccuracy of *in vitro* models is the absence of organ-organ interactions, because cell culture models generally consist of cells from a single organ. For example, drug permeability assay using a monolayer culture of gut epithelial cells (Artursson et al. 2001), or hepatic metabolism models using hepatocytes or liver tissue slices (Alqahtani et al. 2013) provides only partial information about the fate of a drug (Takahashi et al. 2009; Gertz et al. 2010; Prot et al. 2014). Attempts have been made to co-culture gut and liver cells simultaneously. For example, gut cells and liver cells were cultured in separate compartments of a transwell (Choi et al. 2004; Lau et al. 2004; Gonzalez-Arias et al. 2015). Although such a system can realize absorption-metabolism process, several discrepancies from the human body still exist, for example, absence of fluidic flow (Esch et al. 2015; Shemesh et al. 2015), which might affect the transport and reaction of molecules (Kniazeva et al. 2012). Secondly, the liquid-cell ratio in such systems is not physiologically realistic, which may be the cause of inaccurate PK profiles (Sin et al. 2004). Lastly, the relative scaling ratio

between the gut and the liver cells can be an important but yet neglected factor (Moraes et al. 2013; Wikswo et al. 2013).

Due to these limitations of current cell-based models, combination of cell culture technique with microtechnology, often termed organ-on-a-chip technology, has been suggested as alternative models with improved physiological relevance (Sung and Shuler 2012; Sung et al. 2013). Various organ-on-a-chip devices have been developed and reported, including the gut (Sung et al. 2011; Kim et al. 2012; Kim and Ingber 2013; Chi et al. 2015), liver (Lee et al. 2013, 2016), and lung (Huh 2015). An important advantage of organ-on-a-chip technology is the possibility of easily integrating different organ modules on a single chip. Such body-on-a-chip, or multi-organ-on-a-chip devices offer the opportunity of observing multi-organ interaction. Since the early pioneering work by Shuler (Sin et al. 2004; Viravaidya et al. 2004), multi-organ-on-a-chip devices with various combinations of cells have been reported (Mahler et al. 2009; Sung et al. 2010; Esch et al. 2014; Oleaga et al. 2016), with up to 14 different cell compartments (Miller and Shuler 2016). Other research groups have also reported devices with similar concepts (Vozzi et al. 2011; Atac et al. 2013; Maschmeyer et al. 2015).

There are a few examples of multi-organ-on-a-chip devices aimed at reproducing the action of the gut and the liver. Brochot et al. connected cell culture wells with tubes to co-culture gut and liver cells and observed the absorption and metabolism of benzo [a] pyrene (Ouattara et al. 2011). This system demonstrates the preliminary form of connecting the gut and liver cell culture. Leclerc et al. designed a bioreactor that can co-culture gut and liver cells, which was used to predict the clearance parameter of paracetamol (Prot et al. 2014). A PK model was constructed and combined with experimental data to estimate the parameter. One issue is that the PK profile that was observed on chip does not directly reflect the actual *in vivo* PK, which means that although human PK profile can be indirectly predicted by estimating PK parameters such as clearance rate, actual concentration profile that is measured on chip does not match the concentration profile observed *in vivo*.

An attempt to integrate more than one organ module in a single device poses the question of how to set the ratio between the multiple organs. There is a known scaling method that describes the quantitative relationship between different organ sizes in different organisms, such as allometric scaling (Stahl 1965), which has been used to design multi-organ-on-a-chip devices (Ucciferri et al. 2014). Another issue is how to set the flow rate between different organ modules, which affect the rate of transport between the modules. Shuler et al. suggested setting the flow rate to match the residence time in each module to the residence times of corresponding organs in the human body (Sin et al. 2004). Other scaling approaches have also been suggested, for example, a scaling approach that is based on the main physiological function of each organ (Moraes et al. 2013; Wikswo et al. 2013). But despite of these attempts, there has been a lack of consensus on how to design multi-organ-on-a-chip devices.

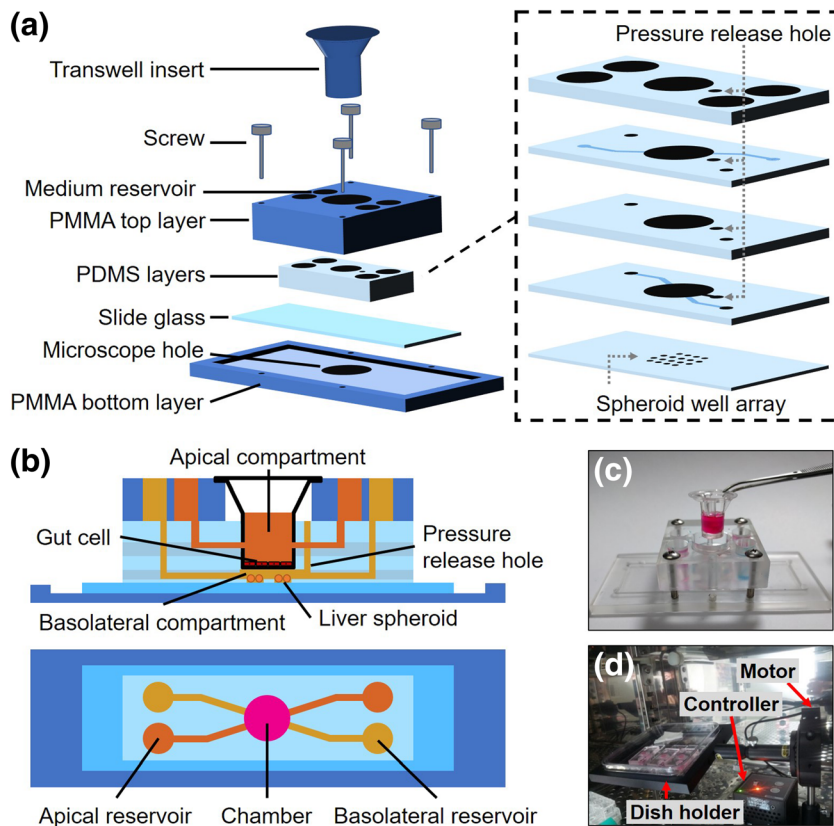
In this study, we designed and fabricated a multi-organ-on-a-chip device for co-culturing gut and liver cells. The main objectives of this study were 1) to develop an easy-to-use, modular multi-organ-on-a-chip device that can co-culture gut and liver cells, and 2) to determine the chip design parameters, including the scaling ratio between the gut and liver cell culture, to achieve a PK profile of a model drug that is similar to that in the human body. To this end, we designed a modular device, which has an insert hole that can snug-fit a commercial transwell insert containing gut cells, and a second layer having a fluidic chamber for liver cells. A PK model of a model drug, paracetamol, was constructed to predict the concentration profile of the drug and its metabolites in the chip, and the model was used to determine the optimal chip design parameters. Our study suggests a useful experimental and mathematical approach for predicting the PK profile of drugs in the body.

## 2 Materials and methods

### 2.1 Fabrication of a gut-liver chip and 3D villi scaffold

The gut-liver chip consists of five polydimethylsiloxane (PDMS) layers and a slide glass sandwiched between two polymethylmethacrylate (PMMA) plates (Fig. 1a and b). The top PMMA plate (W: 40 mm, D: 45 mm, H: 11 mm) contains four medium reservoirs (8 mm diameter) and a hole (16 mm diameter) for a transwell insert. The bottom PMMA plate (W: 95 mm, D: 45 mm, H: 4 mm) contains a 2 mm deep recess that can hold a slide glass. The top and bottom PMMA plates contain screw holes for assembly. The size of all PDMS layers are 4 cm × 2 cm. The first PDMS layer is 2 mm thick with 5 holes, and holds the transwell insert inside the chip. To enable snug-fitting of a transwell insert (Fig. 1c), this PDMS layer was cured inside a dish with a transwell insert. The other four holes were made with a 8 mm diameter biopsy punch. The second PDMS layer is 1.5 mm thick, with three holes and a fluidic channel (W: 200 μm, H: 120 μm) for the apical side. At the center of the second PDMS layer, a 10 mm wide hole is located for a transwell insert. The other two holes are 2 mm wide. The third layer is 1.5 mm thick with three holes, and separates the apical (gut) and basolateral (liver) compartments while holding the transwell insert. The fourth layer is 1 mm thick with three holes (one 8 mm hole in the center and two 2 mm hole at corners, for connection to fluidic channels), and contains a fluidic channel for basolateral (liver) compartments (W: 200 μm, H: 120 μm). For the top four PDMS layers, we made additional, small pressure-release hole that is 2 mm in diameter, near the center area. This pressure-release hole is necessary to prevent backflow when a transwell insert is pushed into the chip. The last, fifth layer provides a space for holding liver spheroid culture. It is 300 μm thick and contains an array of eighteen 1 mm-holes, so that spheroids can settle inside the holes. The transwell insert needs to be modified slightly to enable perfusion cell culture. A 32G SUS-pipe with 0.235 mm outer diameter was heated with flame, and was

**Fig. 1** **a** Schematic illustrations of the gut-liver chip. **b** Side and top view of a gut-liver chip **c** A picture of a gut-liver chip. **d** A picture of gravity flow machine in incubator



used to punch two opposing holes on the sidewall of an insert. To assemble the chip, the slide glass and the PDMS layers were treated with air plasma (CUTE vacuum plasma cleaner, Femto Science, Korea) at 70 watts for 30 s, and bonded sequentially. The bonded PDMS layers were fixed between the PMMA plates with screws. The 3D villi structure was fabricated following the methods from our previous paper (Sung et al., 2011). To briefly explain, a wafer mold with the inverse structure of the villi was fabricated using photolithography technique. A SU-8 mold with the villi structure was replicated from the wafer mold, and bonded to a gasket to make the alginate inverse mold. Finally, collagen(CB354249, Corning) villi scaffold was replicated from the alginate mold, which was then dissolved. The fabricated collagen villi structure was bonded to a porous membrane inside the transwell insert, using collagen as a glue.

## 2.2 Cell culture on chip

For gut cells, we used human colon carcinoma cell line, Caco-2, and for liver cells, we used hepatoma cell line, HepG2 (obtained from American Type Culture Collection (ATCC)). A high glucose DMEM (Dulbecco's Modified Eagle's Medium) with 10% FBS and 1% penicillin-streptomycin (Welgene) was used to culture both cells. Cells were incubated in a cell culture incubator, maintained at 37 °C with 5% CO<sub>2</sub>. A suspension of  $4 \times 10^4$  Caco-2 cells were seeded to a transwell insert and grown for 7 days in a cell culture incubator. After 7 days, the transwell insert was

transferred to a chip. To culture HepG2 cells as spheroids, previously reported methods were followed (Lee et al. 2013). Concave microwells was coated with 3% BSA solution for 1 h, and 1 ml of HepG2 cell suspension at  $5 \times 10^5$  cells/ml was seeded into the microwells. After 4 days of culture in microwells, spheroids were transferred to a gut-liver chip. There were approximately  $7 \times 10^3$  cells were present in a single spheroid. The diameter of each spheroid was approximately 300 μm, mostly ranging from 250 to 350 μm. Each hole in the microfluidic device contained about four spheroids which stayed in place during perfusion. To culture HepG2 as a monolayer,  $4.5 \times 10^4$  HepG2 cells were seeded directly to a gut-liver chip and cultured on chip for 4 days. Media was changed every 2 days for Caco-2 and everyday for HepG2. A gut-liver chip was operated using a custom-made gravity flow device (Fig. 1d). The details of the gravity flow device is provided elsewhere (Kim et al. 2013). The operating condition was set as 0.1 degrees/s, and a tilting angle of 10 degrees, and remained in each position for 500 s.

## 2.3 Fluid dynamics simulation

COMSOL Multiphysics® software was used to model the flow velocity and shear stress inside a gut-liver chip. A laminar flow module was used to reconstruct the geometry of the chip except the reservoir. The inlet velocity was set as  $4.6 \times 10^{-3}$  m/s, based on experimental observation, and the

outlet pressure was set as 0 Pascal. For simplicity, fluid dynamic properties of water were used throughout the model.

## 2.4 Visualization of cell morphology

The morphology of Caco-2 cells were examined by staining the actin and nuclei of the cells. First, cells were washed once briefly with DPBS and fixed with 4% (*w/v*) paraformaldehyde (Sigma, 158,127) for 1 h. Then, the cells were washed three times with 0.1% BSA solution (Gibco, 30,063) for 5 min. To permeabilize the cell membrane, cells were treated with 0.3% (*w/v*) Triton-X 100 (Junsei, 49,415–1601). Nuclei were stained for 30 min with Hoechst 33,342 (Invitrogen, H3570), diluted at 1/600 ratio in DPBS, followed by washing with DPBS for 5 min. To stain actin, Rhodamine Phalloidin (Sigma, P1951) was diluted at 1/100 ratio in DPBS and cells were treated for 90 min, followed by 5 min of DPBS washing. Stained cells were examined with confocal laser scanning microscope (Carl Zeiss, LSM700).

## 2.5 Measurement of cytochrome P450 activity

Measurement of P450 activity was made after 4 days of culture in the chip. Vivid BOMCC substrate (Life Technologies, P2975) was used to measure the activity of cytochrome P450 enzyme activity of liver cells. BOMCC is known to be a substrate of P450 3A4 and 2C9 (Brahmi et al. 2012). The Vivid BOMCC substrate was diluted at 1/10 ratio and inserted into the basolateral side of the chip (liver layer). After incubation for 30 min at 25 °C, 200 μL was transferred to a 96-well microplate (Corning 3631). Fluorescent intensity was measured using Cary Eclipse Fluorescence spectrophotometer (Agilent) at excitation wavelength of 460 nm and emission wavelength of 495 nm. After measuring the P450 activity, the number of cells was quantified by trypsinizing the cells and staining with Trypan blue. HepG2 spheroids were also segregated by trypsinization for cell counting. All statistical analysis was performed using Student-t test to obtain statistical significance.

## 2.6 Measurement of paracetamol metabolites

The concentrations of paracetamol and its metabolites were measured with a HPLC (Younglin Science, YL9100 HPLC system, Korea). Paracetamol in cell culture media at 2 mM concentration was inserted into the apical compartment (gut layer). The basolateral compartment (liver layer) was filled with fresh media. After 6 and 24 h, 100 μL of samples were taken from each side. Metabolic reaction was terminated by adding 50 μL of methanol and the samples were stored at -80 °C until analysis. The samples were centrifuged at 300 RPM for 10 min, and the supernatant was filtered with syringe filter (Thermo, 4-SF-45(RC)). A Polaris C18-A column with

250 mm length, I.D. 4.6 mm, particle size 5 μm (Agilent) was used. Two mobile phases were used; solvent A (distilled water) and solvent B (acetonitrile) at flow rate of 0.3 ml/min. Solvent composition was 5% B (0–2 min), 5% - 100% B (2–22 min), 100% B (22–26 min), 100% - 5% B (26–26.1 min), and 5% B (26.1–40 min). Sample injection volume was 40 μL, and detection was made using UV/vis detector (wavelength 280 nm). The concentrations of paracetamol and its metabolites were determined by drawing a standard curve with known concentrations of each compound (Paracetamol (Sigma, A7085), paracetamol sulfate potassium salt (Sigma, 89,604), and paracetamol β-D-glucuronide (Sigma, 43,073)).

## 2.7 Pharmacokinetic modeling

A pharmacokinetic (PK) model describing the transport and reaction of paracetamol in the gut-liver chip was constructed. The PK model consists of three compartments (apical, Caco-2 and basolateral compartments, Fig. 2a). Several parameters were used to describe the rate of transport and reactions, which are summarized in Supplementary Information file. The parameters were fitted to experimental data at certain time points, using MATLAB nonlinear least-squares curve fitting function. First, model parameters were fitted using data from a well-plate experiment. Then the constructed PK model was compared with known human PK of a same drug. The model parameters were further modified to improve the gut-liver chip PK (Fig. 2b).

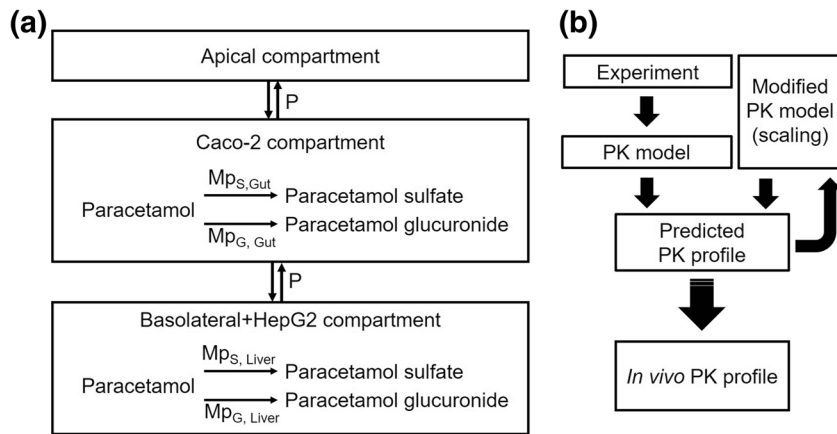
## 3 Results

### 3.1 Chip design and fluid dynamics simulation

The microfluidic gut-liver chip consists of two PDMS layers, gut (apical) and liver (basolateral) layers (Fig. 1a and b). The size of the center hole in the gut layer was carefully adjusted so that a commercially available transwell insert can snug fit into the hole (Fig. 1c). Holes for medium perfusion were located in opposite locations on the side of the transwell. The main advantage of this chip is that gut cells can be cultured either on chip or separately in a transwell, which can be transferred to the chip later. A liver layer is located directly below the gut layer, separated by a porous membrane. The liver layer can also accommodate either 2D monolayer culture of liver cells, or 3D culture of liver cells. The base of the liver layer contains an array of holes that are intended for holding liver cells in 3D forms, such as spheroids. Using this chip, we were able to culture Caco-2 cells up to 3 weeks, and Caco-2 and HepG2 cells were co-cultured for up to 5 days in the chip (Choe et al. 2017).

Flow was introduced by using a computer-controlled gravity flow machine (Fig. 1d) (Kim et al. 2013). At a fixed tilting

**Fig. 2** Schematic diagram of PK model and experiment procedure. **a** PK model compartments and parameters. **b** Experiment and scaling procedure



angle of 10 degrees, the flow rate measured in the gut compartment was  $6.6 \mu\text{L}/\text{min}$ , whereas the flow rate in the liver compartment was measured to be  $4.3 \mu\text{L}/\text{min}$  (Fig. 3a). The velocity and shear stress near the membrane, where gut cells are cultured, were analyzed by fluid dynamics simulation using COMSOL Multiphysics®. The line A-A' shows a direction that is parallel to the direction of the flow, and the line B-B' shows a direction that is perpendicular to the direction of the flow (Fig. 3b). The location of channels within the chip was an important design parameter, since a channel that is too near to the cell culture area might result in too high shear stress, whereas a channel that is too far might result in mass transfer limitation. Simulation results show that at the center of the membrane, the fluid velocity was predicted to be  $1 \times 10^{-5} \text{ cm/s}$ ,  $1 \times 10^{-6} \text{ cm/s}$ , and  $1 \times 10^{-8} \text{ cm/s}$ , with channels located at 1, 3, and 5 mm higher than the membrane, respectively (Fig. 3c and d). The shear stress was predicted to be  $1 \times 10^{-4} \text{ dyne/cm}^2$ ,  $4 \times 10^{-5} \text{ dyne/cm}^2$ , and  $2 \times 10^{-8} \text{ dyne/cm}^2$ , with channels located at 1, 3, and 5 mm higher than the membrane, respectively (Fig. 3e and f). This result shows that the fluid dynamics profile was highly sensitive to the location of channels, and both velocity and shear stress dramatically decreased with an increasing distance of channel location from the membrane. Simulation results also show that velocity and shear stress tend to decrease at certain locations. This was mainly caused by the backflow created inside the cell culture chamber (see *Supplementary Information*). Based on the simulation results, we determined the location of the channel to be 3 mm higher than the membrane, so that a moderate velocity and shear stress are maintained without excessive backflow.

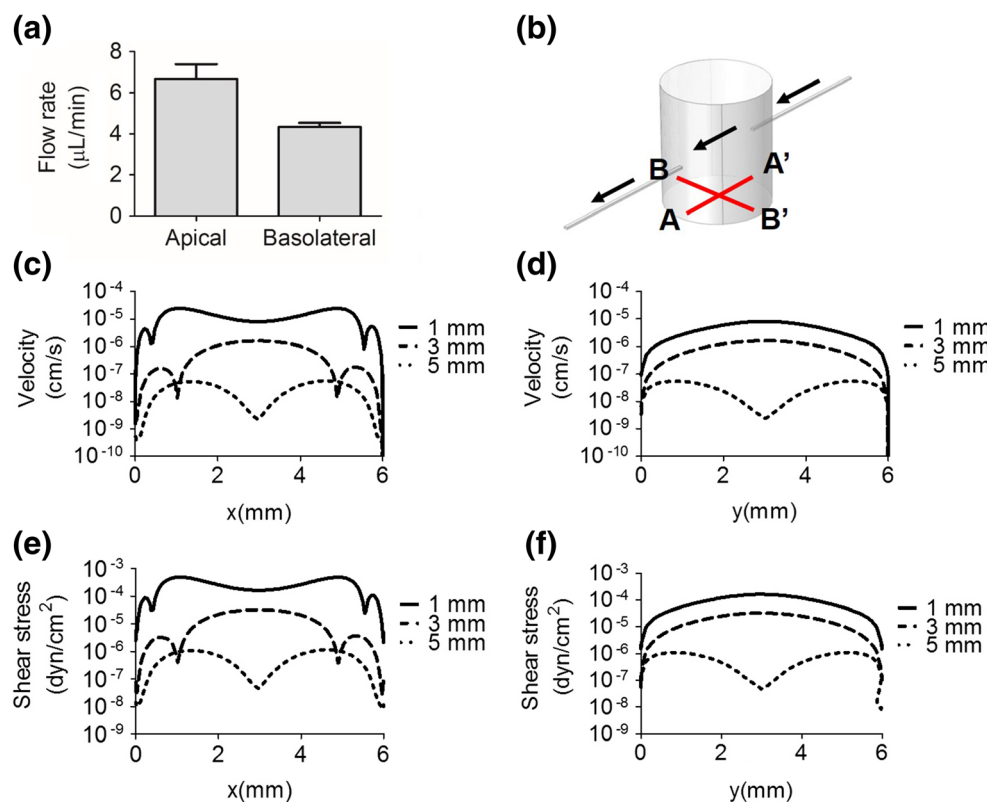
### 3.2 Analysis of gut and liver cells in the chip

Our gut-liver chip is compatible with both 2D and 3D culture format in both gut and liver compartments. To illustrate both 2D and 3D cell culture in the chip, we cultured Caco-2 cells in both 2D and 3D format. For 2D cell culture, a standard culture

protocol was followed (Artursson et al. 2001), where Caco-2 cells were seeded on top of a porous membrane in a transwell insert and cultured for 2 weeks in monolayer. For 3D cell culture, we followed the methods from our previous paper using collagen villi scaffold (Sung et al. 2011; Kim et al. 2013). After 2 weeks, the morphology of the cells was analyzed with confocal microscopy and H & E staining. In case of 2D culture in the chip, Caco-2 cells formed a uniform monolayer on the membrane (Fig. 4a-d). Polarization of the cells was confirmed by the localization of actin near the membrane. In case of 3D culture, cells formed a monolayer conforming to the collagen villi scaffold, making a 3D shape resembling the intestinal villi (Fig. 4e). Cells formed a uniform monolayer around the collagen villi both at bottom region (Fig. 4f), and top region (Fig. 4g). Polarization of cells was also confirmed, as nuclei of the cells were located near the collagen scaffold, and actin was more strongly expressed on the outer side of the cell layer. The shape of the cells was also generally in columnar shape, which indicates differentiation of Caco-2 cells. Tissue morphology was also examined, by H & E staining of both 2D and 3D culture of Caco-2 cells. H & E stain of Caco-2 cells in 2D monolayer also confirms proper polarization of the cells, with localization of cell nuclei near the bottom membrane, and formation of a tight barrier on top (Fig. 4h). In case of 3D culture, H & E staining shows a formation of cell layer around the collagen villi scaffold (Fig. 4i).

We also attempted both 2D and 3D cultures of liver cells in the chip. For liver cells, hepatocarcinoma cell line, HepG2, was used. For 3D cell culture, spheroids were formed according to a method in previously reported study using concave microwells (Lee et al. 2013), and then seeded into the liver compartment the same way as the 2D culture. To prevent the spheroid particles from washed away by fluidic shear, an array of holes was fabricated at the bottom surface of the liver compartment. When injected, spheroids travel through channels and settle inside the holes (Fig. 5a). Cytochrome P450 enzyme is one of the major metabolic enzymes expressed in the liver

**Fig. 3** Flow characteristics inside the gut-Liver chip. **a** Flow rate of gut-liver chip. **b** Schematic diagram of gut chamber of the gut-liver chip. Velocity profile of apical compartment of the gut-liver chip **c**, in x-axis, and **d**, in y-axis. **e** Shear stress profile of apical compartment of the gut-liver chip in x-axis, and **f**, in y-axis. In the figures, the direction of x-axis is parallel to A-A' and the direction of y-axis is parallel to B-B' direction



tissue, but is often poorly expressed in the *in vitro* cell models (Donato et al. 2008). BOMCC is a known to be a substrate of P450 3A4 and 2C9 enzymes (Brahmi et al. 2012). Figure 5b shows the P450 enzyme activity measured when cells were cultured in different conditions. Results show a significant increase of per cell enzyme activity when HepG2 cells were in 3D spheroids (3D well,  $8.86 \times 10^{-7}$  mol/ $10^{10}$  cells/h), compared to monolayer (2D well, not detected). Culturing the cells in a chip enhanced P450 enzyme activity significantly. When they were cultured in 2D monolayer in a chip (2D chip), P450 activity was measured at  $4.60 \times 10^{-6}$  mol/ $10^{10}$  cells/h, and when they were cultured in 3D spheroids in a chip (3D chip), P450 activity was highest ( $1.21 \times 10^{-5}$  mol/ $10^{10}$  cells/h). These results show that both culturing cells in 3D spheroids and culturing cells in a fluidic environment enhances the cell's metabolic activity, possibly having synergistic effect. For all of following chip experiment, HepG2 cells were cultured in 3D spheroids.

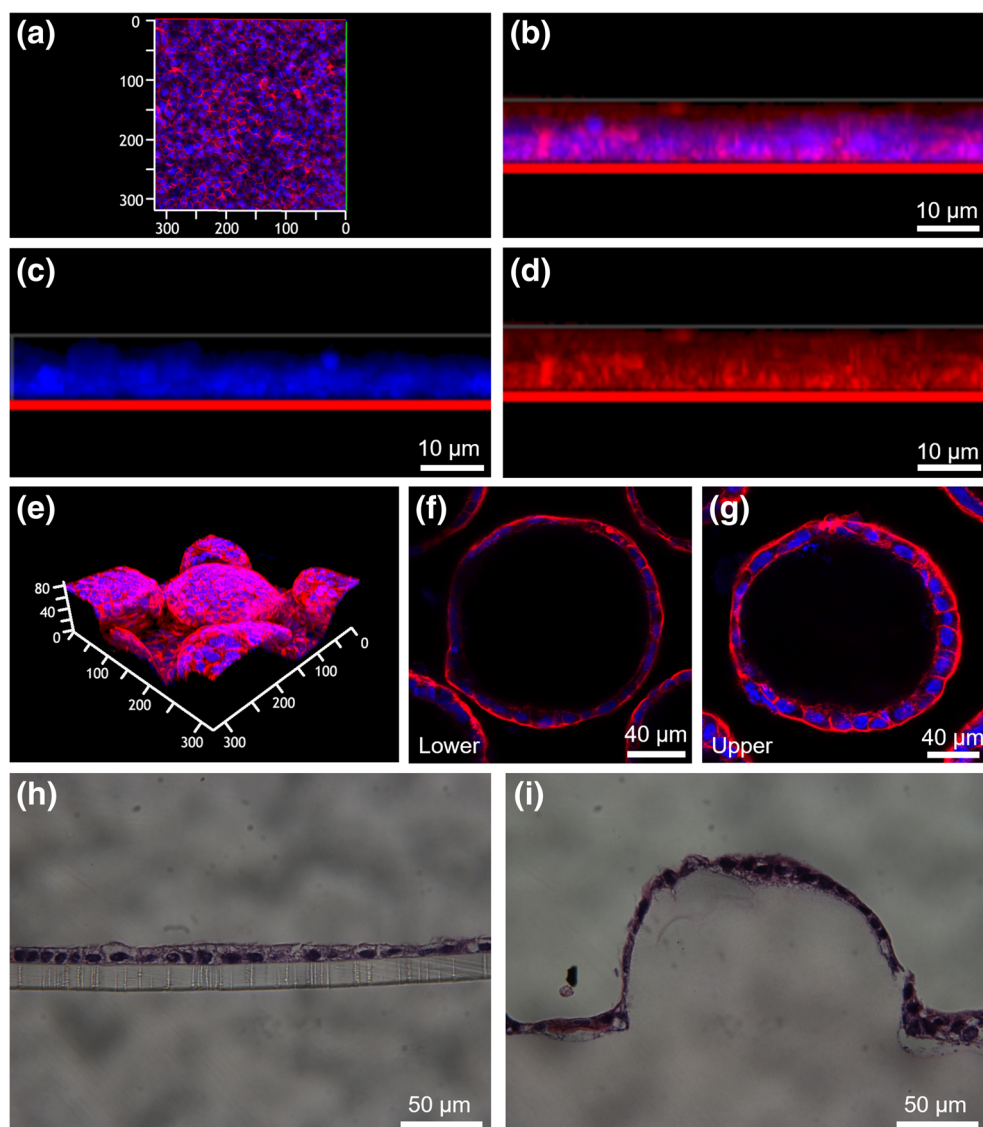
HepG2 spheroids were incubated in a chip, and the P450 enzyme activity was measured at various incubation times. Figure 5c shows that HepG2 spheroids maintained relatively constant metabolic activity at  $1.2 \times 10^{-5}$  mol/ $10^{10}$  cells/h during the 10-day culture period, with a slight decrease in the activity noted at day 10. Based on this result, all subsequent experiment was performed with spheroids that had been incubated for 4 days. To verify if it is possible to control the total metabolic activity of the liver module by changing the number

of spheroid particles, we measured the activity of P450 enzyme at varying number of spheroid particles ranging from 20 to 100 (Fig. 5d). Increasing the number of spheroid particles resulted in a linear increase in the total number of product (BOMCC) molecules formed, from  $2.47 \times 10^{-12}$  mol at 20 spheroid particles to  $2.02 \times 10^{-11}$  mol at 100 particles.

### 3.3 Construction of PK model and scaling the gut-liver chip

A pharmacokinetic (PK) model of the gut-liver chip was constructed, using paracetamol as a model drug. Our approach was to construct a PK model of a chip based on the size of each compartment (gut and liver), and derive necessary kinetic parameters from separate, well-based experiment using gut and liver cells. For parameters related to the absorption and metabolism in the gut, Caco-2 cells were cultured in a transwell plate, and concentrations of paracetamol and its metabolites were measured in apical and basolateral sides of the transwell (See [Supplementary Information](#) for details on parameter fitting using Caco-2 and HepG2 cells in a transwell). The fitted parameter for absorptive permeability of paracetamol was  $1.04 \times 10^{-1}$  cm/h, whereas the absorptive permeabilities of paracetamol sulfate and paracetamol glucuronide were  $4.99 \times 10^{-2}$  cm/h and  $5.89 \times 10^{-2}$  cm/h, respectively. The metabolic activity of Caco-2 cells was found to be  $14.9 \text{ h}^{-1}$

**Fig. 4** Confocal microscope image of Caco-2 cells on membrane after staining for actin (red) and nucleic acid (blue). **a** Top-down view and **b, c, d**, cross sectional views. Panel **b** is merged image of **c** and **d**. Confocal microscope image of Caco-2 cells on 3D collagen villi scaffold. **e** After 3D rendering and cross sectional views at the **f**, upper and **g**, lower side of the villi. H&E stained images of the Caco-2 cells on membrane **h**, and **i**, 3D collagen villi scaffold.A



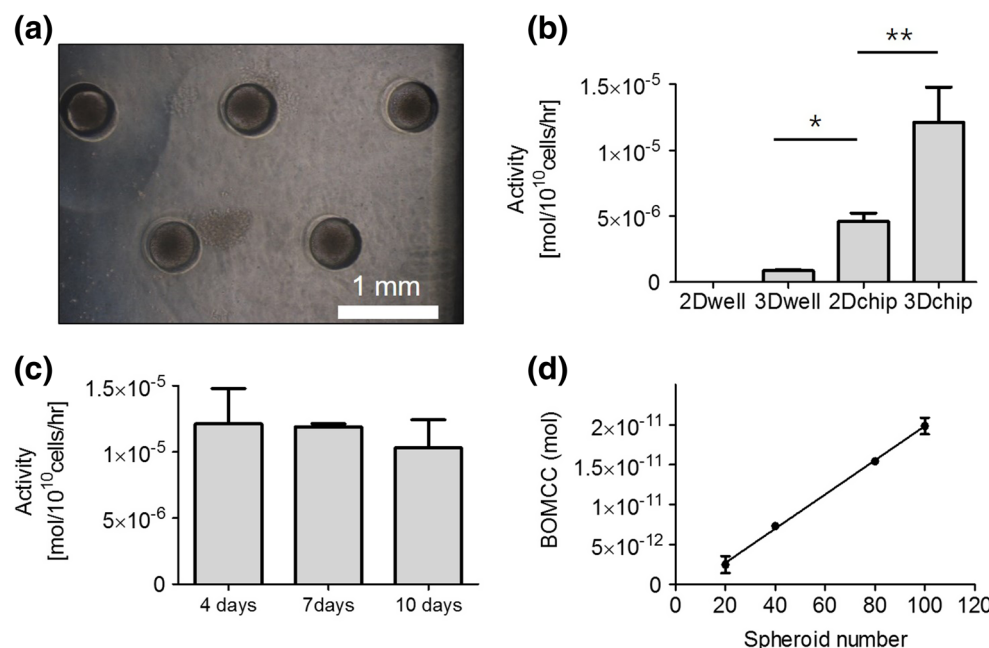
for sulfation reaction, and  $17.6 \text{ h}^{-1}$  for glucuronidation reaction.

To obtain parameters related to the metabolism in the liver, HepG2 cells were cultured in a microwell plate, and concentrations of paracetamol and its metabolites were measured at 6 and 24 h. The fitted metabolic rate of HepG2 cells was  $0.35 \text{ h}^{-1}$  for sulfation reaction, and  $0.59 \text{ h}^{-1}$  for glucuronidation reaction. All of the fitted parameters are summarized in Table 1. These parameters were used to construct a PK model of paracetamol in the gut-liver. In Fig. 6, predicted concentration profiles in the apical (gut layer) and basolateral (liver layer) sides were compared with data obtained from chip experiment. As shown in the figure, parameters derived from well-experiments provided a reasonably good fit against concentration data from the gut-liver chip. One limitation of our study is that we were able to obtain only two data points for

each condition, due to the limitation of analytical technique and the amount of sample required.

We compared major pharmacokinetic parameters with the known *in vivo* PK parameters in humans. The parameters we examined were a peak time, peak concentration, and half-life time. The predicted PK parameters for the gut-liver chip and known PK parameters from humans are summarized in Table 2, and the simulation result is shown in Fig. 7a. The peak time was estimated to be approximately 25.6 h in the gut-liver chip, which was significantly longer than the *in vivo* parameter ( $0.5 \sim 2 \text{ h}$ ) (Zurlinden and Reisfeld 2016). The peak concentration was estimated to be  $646.2 \mu\text{M}$  in the gut-liver chip, whereas in humans, the peak concentration is expected to be approximately  $200 \mu\text{M}$  (Zurlinden and Reisfeld 2016). Half-life time also showed significant deviation;  $63.2 \text{ h}$  in the gut-liver chip, compared to  $1 \sim 4 \text{ h}$  in humans. These

**Fig. 5** **a** A differential interface contrast microscope image of HepG2 spheroid in concave microwell arrays. **b** Specific activity of CYP450 3A4 enzyme in HepG2 cells cultured in various condition. 2D means monolayer culture condition and 3D means spheroid culture condition. **c** Specific activity of CYP450 3A4 enzyme in HepG2 spheroid change with culture days. **d** Total activity of CYP450 3A4 enzyme in HepG2 spheroid change with the spheroid numbers. A symbol (\*) denotes  $p < 0.05$  and (\*\*) denotes  $p < 0.01$



discrepancies led us to set up a hypothesis that the gut absorption and liver metabolism are not occurring at sufficiently high rate in the gut-liver chip. Therefore, we speculated that by modifying chip design parameters to compensate these shortcomings, we may be able to improve the PK profile. The parameters we modified were 1) gut absorptive surface area, which determines the absorption rate of paracetamol, and 2) liver cell volume, which determines the total metabolic rate in the liver compartment. First, we tested the effect of changing the two parameters independently (Supplementary Information). We could observe that increasing the liver volume contributed to the lower peak concentration, and increasing the gut surface area contributed to shorter peak-time and half-life time. Increasing the two parameters simultaneously resulted in a shorter peak time and half-life time, but no significant change in the peak concentration (Fig. 7b and Table 2). More specifically, the peak time decreased to 0.4 h (close to the *in vivo* value of 0.5 to 2 h), and half-life time decreased to 3.2 h (close to the *in vivo* value of 1 to 4 h). The peak concentration, however, did not change significantly, as it was predicted to be 680.5  $\mu\text{M}$ , which is higher than the *in vivo* value of 200  $\mu\text{M}$ . However, simulation results suggest that it is at least possible to improve a PK profile in the gut-liver chip, close to the human PK.

#### 4 Discussion

The gut-liver chip was designed so that a commercially available transwell insert can snug-fit into an open hole. This allows flexible culture conditions, where one can either culture gut cells separately in a transwell until full differentiation and transfer them into the chip, or culture them in the chip from early stages, exposing the cells to flow (Chi et al. 2015). Fluid dynamics simulation shows that cells can be exposed to varying levels of fluidic shear, by adjusting the location of fluidic inlet and outlet holes on the side walls of the transwell insert (Fig. 3). In our study, we fixed the location of the fluidic holes to be 3 mm higher than the membrane, resulting in the shear stress of  $4 \times 10^{-5}$  dyn/cm<sup>2</sup>, which is smaller than the fluidic shear stress reported in previous studies. Ingber group used a flow rate of 30  $\mu\text{L}/\text{h}$ , corresponding to a shear stress of 0.02 dyn/cm<sup>2</sup> (Sin et al. 2004), whereas Chi et al. reported culturing Caco-2 cells under varying shear stress from  $4 \times 10^{-4}$  to  $2 \times 10^{-3}$  dyn/cm<sup>2</sup>, without apparent detrimental effect on cell viability or functions (Chi et al. 2015). Based on these studies, the fluidic condition used in our study seems to be appropriate for Caco-2 cell culture.

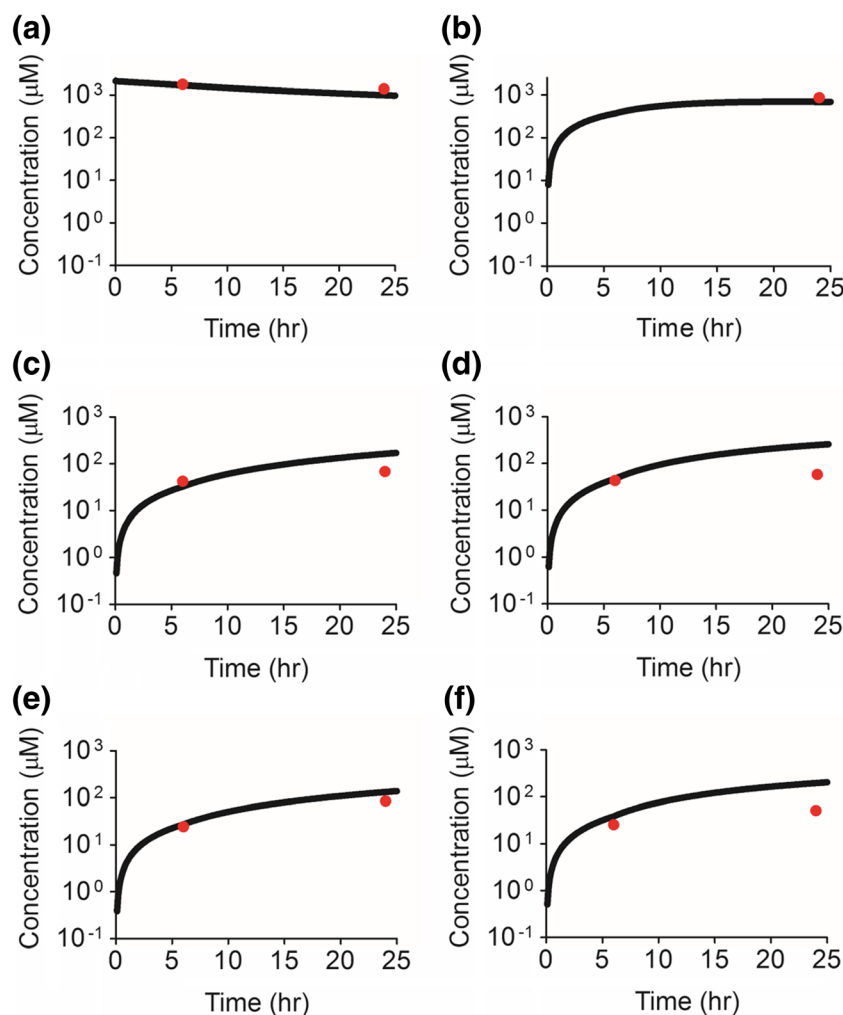
In a well-plate environment, Caco-2 cells are differentiated after 21 days of culture (Artursson et al. 2001; Alqahtani et al.

**Table 1** Fitted PK model parameters

Parameter	P <sub>Para</sub> ( $10^{-3}$ cm/h)	P <sub>Sulf</sub> ( $10^{-3}$ cm/h)	P <sub>Glu</sub> ( $10^{-3}$ cm/h)	M <sub>p</sub> <sub>S,Gut</sub> (hr <sup>-1</sup> )	M <sub>p</sub> <sub>G,Gut</sub> (hr <sup>-1</sup> )	M <sub>p</sub> <sub>S,Liver</sub> (hr <sup>-1</sup> )	M <sub>p</sub> <sub>G,Liver</sub> (hr <sup>-1</sup> )
Value	103.8	49.9	58.9	14.9	17.6	0.35	0.59

The symbol ‘P’ denotes absorptive permeability, and the symbol ‘Mp’ denotes metabolic activity. Subscript ‘Para’ denotes paracetamol, ‘Sulf’ denotes paracetamol sulfate, and ‘Glu’ denotes paracetamol glucuronide. M<sub>p</sub><sub>S,Gut</sub> and M<sub>p</sub><sub>G,Gut</sub> denote sulfation and glucuronidation activity of gut (Caco-2) cells, respectively. M<sub>p</sub><sub>S,Liver</sub> and M<sub>p</sub><sub>G,Liver</sub> denote sulfation and glucuronidation activity of liver (HepG2) cells, respectively

**Fig. 6** PK profile of paracetamol in the gut-liver chip. Experiment data and model-predicted concentrations of paracetamol in **a**, apical compartment and **b**, basolateral compartment. Experiment data and model-predicted concentrations of paracetamol glucuronide in **c**, apical compartment and **d**, basolateral compartment. Experiment data and model-predicted concentrations of paracetamol sulfate in **e**, apical compartment and **f**, basolateral compartment. The circles are measured experiment data. The line is simulation result of well experiment-based model



2013). In our study, Caco-2 cells were cultured in the chip for up to 14 days before analysis. When cell morphology was analyzed, we could verify that the cells were reasonably well polarized, and tight junctions were properly formed. It has been reported that culturing Caco-2 cells in a fluidic environment induces quicker differentiation than the static culture condition (Kim et al. 2012; Yu et al. 2012; Kim and Ingber 2013; Chi et al. 2015). It is interesting that culturing cells in a fluidic condition also enhances the overall functionality of the cells, for example mucin production (Chi et al. 2015), and expression of differentiation marker (Kim et al. 2012; Kim and Ingber 2013; Shim et al. 2017), and attachment of microbiotics (Costello et al. 2014).

Cytochrome P450 enzymes are major hepatic metabolic enzymes, classified as phase I enzymes (Westerink and Schoonen 2007). Metabolism of paracetamol involves several enzymes, including CYP 1A2, 2E1, and 3A4 (McGill and Jaeschke 2013). We measured the activity of P450 enzyme of HepG2 cells to evaluate the metabolic function of the cells in various conditions. Although HepG2 cells are a widely used *in vitro* liver model, one of the critical disadvantages of

HepG2 model is almost negligible expression of P450 enzymes (Westerink and Schoonen 2007; Donato et al. 2008). In particular, P450 3A4 is known to be poorly expressed in HepG2 cells (Wilkening et al. 2003). Improved expression of P450 3A4 indicates that the metabolic function of HepG2 cells was enhanced in microfluidic chip (Fig. 5). It has been reported that culturing HepG2 cells in 3D matrix such as collagen or Matrigel can enhance metabolic activity of the cells (Westerink and Schoonen 2007; Ramaiahgari et al. 2014). Exposing HepG2 cells to fluidic shear is also known to enhance the metabolic activity of the cells (Baudoin et al. 2011). Although the mechanism is not well known, it might be related to the enhanced convective mass transfer. It is interesting to note that the effect of combination of the two factors, fluidic shear and 3D spheroid, exerted synergistic effect.

One of the key issues in constructing a multi-organ chip is how to scale different organs with respect to each other (Moraes et al. 2013; Wikswo et al. 2013). In particular, relative scaling of the gut and the liver module can profoundly affect the PK and pharmacological effect of administered drugs. Although several approaches for scaling multi-organ

**Table 2** Scaling parameters and predicted PK parameters of PK model for Reproducing *in vivo* PK(pharmacokinetic) Profile

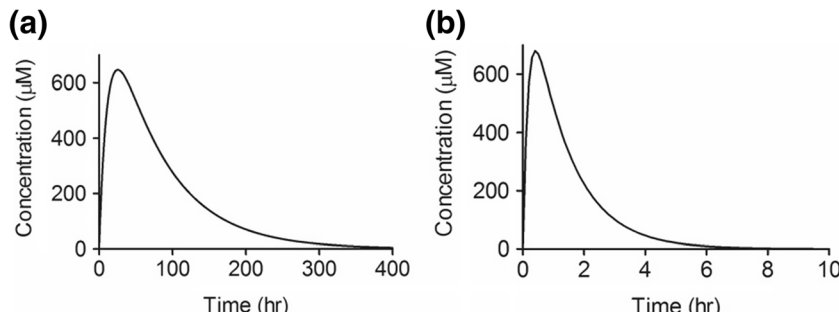
		<i>in vivo</i> parameters (scaled)	Original chip parameters	Dimension-corrected parameters Gut surface area + Liver tissue volume
Scaling parameter	Apical volume ( $\mu\text{L}$ )		500	500
	Gut surface area ( $\text{cm}^2$ )	30(Helander and Fandriks 2014) $\text{m}^2$ (22.8 $\text{cm}^2$ )	0.33	22.8
	Basolateral volume ( $\mu\text{L}$ )	5(Davies and Morris 1993) L (380 $\mu\text{L}$ )	380	380
	Liver tissue volume ( $\mu\text{L}$ )	1.13(Davies and Morris 1993; Sweeney, Shuler et al. 1995; Sin, Chin et al. 2004) L (85.6 $\mu\text{L}$ )	3.43	85.6
Predicted PK parameter	peak time (hr)	0.5~2(Zurlinden and Reisfeld 2016)	25.6	0.4
	peak concentration ( $\mu\text{M}$ )	198(Zurlinden and Reisfeld 2016)	646.2	680.5
	Half-life time (hr)	1~4(Zurlinden and Reisfeld 2016)	63.2	1.1

The gray shaded parameters are modified towards *in vivo* ratio

chips have been suggested (Moraes et al. 2013; Wikswo et al. 2013; Ucciferri et al. 2014; Abaci and Shuler 2015), there has been no consensus on methods of scaling the chip. One scaling method is allometric scaling, which uses the power law to

deduce relationship between organ sizes or functions and the mass of an organism (Stahl 1965). Alternatively, Shuler et al. have proposed scaling different organs based on blood residence times in corresponding organs (Sin et al. 2004). Other,

**Fig. 7** PK profile of paracetamol in basolateral compartment with **a.** original chip parameter model, and **b.** dimension-corrected parameter model



more sophisticated methods of scaling have also been proposed, for example, one can scale different organ modules based on their functions, which can roughly be classified into 2D-based and 3D-based functions (Moraes et al. 2013; Wikswo et al. 2013). Another approach to predict the PK of drugs using an organ on a chip was recently proposed (Prot et al. 2014; Bricks et al. 2015). Mathematical models, such as well-stirred model or parallel tube model, that simulate the transport and reaction of drugs in the chip are used to estimate the clearance rate from the chip data, which can then be converted to predict human PK.

One of the objectives of this study was to examine if known PK of a drug in human body can be reproduced in the gut-liver chip. Reproducing the actual human PK is important because the gut-liver chip can be used for, not only predicting the PK of a drug, but also for evaluating the drug's effect on target organs. Exposing target organs to accurate concentrations of drugs and their metabolites is essential for obtaining realistic responses (Sung et al. 2013, 2014). Experimental data from the gut-liver chip and PK model simulation suggested that the predicted PK profile of paracetamol showed considerable deviation from known human PK.

The primary reason for this deviation in observed PK of paracetamol in the chip compared to that in human is the insufficient metabolic capacity of HepG2 cells. Literature suggests that expression levels of various metabolic enzymes are very different between HepG2 cell line and primary hepatocytes (Wilkening et al. 2003). For example, mRNA expression of CYP 2E1 is about 1460 times higher in primary hepatocytes compared to HepG2 cells. In case of UGT enzyme, hepatocytes showed 22 times higher expression than HepG2 cell line. In case of SULT enzyme, hepatocytes showed 3 times lower expression than HepG2 cell line. Combining these figures, we could anticipate increased glucuronidation and reduced sulfation if we used primary hepatocytes instead of HepG2 cell line. We hypothesized that the another cause of this deviation were an insufficient gut surface area, and low capacity of hepatic metabolism. This hypothesis was based on the ratio between the liver volume, gut surface area, and total blood volume. In humans, average gut surface area is 30 m<sup>2</sup> (Helander and Fandriks 2014), the total volume occupied by hepatocytes is 1.13 L (Davies and Morris 1993; Sweeney et al. 1995; Sin et al. 2004), and the total blood volume is 5 L (Davies and Morris 1993). This results in the ratio of 0.6: 1: 0.23 (gut surface area: blood volume: liver volume), when normalized with respect to the blood volume. Compared to this, the ratio in the gut-liver chip is calculated to be  $8.68 \times 10^{-4}$ : 1:  $4.74 \times 10^{-3}$ , when assuming the volume media in the chip as the blood volume. This shows that the size of gut and the liver compartment in the gut-liver chip is considerably underestimated compared to the blood volume. Modification of gut absorptive area and liver cell volume, significantly enhanced the PK profile in the chip (Fig. 7b). Another important

factor that determines the PK of paracetamol in humans is the rate of gastric emptying (Raffa et al. 2014), but this is not realized in our gut-liver chip. Incorporation of a stomach module to realize gastric emptying might help the gut-liver chip realize the PK profile that resembles the PK in humans.

We realize that our study still carries several limitations. For example, the drug concentration used in our study far exceeds the actual dose or plasma concentrations in humans. This was mainly because of the detection limit of analytical methods used in our study, as well as the limitation of sampling volumes. Excessive dosing of the drug may have saturated the transporters and metabolic enzymes, affecting the observed PK. Another limitation is that we only used one model drug, which does not necessarily cover other drugs with vastly different chemical properties. It is probably necessary to repeat a series of studies similar to this for a line of drugs with different properties. Another factor that needs consideration is the extent of surface binding. Paracetamol is fairly hydrophobic compound and there is a possibility of surface binding and consequent loss of significant fraction of original dose. In face we observed significant loss of molecules in our previous study and tested several pre-treatment methods to minimize surface binding (Lee et al. 2017). Surface binding seemed to have affected the result of our P450 experiment using spheroids. Some inconsistencies were noted at lower spheroid number, and we speculate that this might be because of some nonspecific binding of BOMCSS product inside the device.

Although this work focuses on the first-pass metabolism, which is essentially realized by the action of the two organs, gut and liver, our gut-liver chip can be easily adapted to other situations where multiple organs are involved. For example, gut, liver, pancreas, muscle, and brain work in concert to regulate the glucose metabolism in the body (Bergman 2007), and the gut plays a central role in the functions of distant organs such as the brain and the skin, which are often termed as gut-brain axis, and gut-skin axis (O'Neill et al. 2016; Scott et al. 2017). Our gut-liver chip can simply replace gut or liver cell culture with other cell types to realize different versions of the chip, making it potentially useful as a modular platform for studying various inter-organ actions.

## 5 Conclusion

In this study, we developed a modular gut-liver chip for co-culturing gut and liver cells in both 2D and 3D configurations. A model drug, paracetamol, was used to study the PK in the chip and compare it with a known PK in humans. The original gut-liver chip design resulted in significantly slow clearance of the drug, which was partially improved when gut absorption surface area and liver cell volume were increased. Our microfluidic gut-liver chip, combined with PK modeling, may

provide a novel platform and strategy to study the first-pass metabolism of various drugs. Not only this, our chip can potentially be useful for culturing any two independent tissues or cells and studying the dynamics of interaction between them.

**Acknowledgments** This work was supported by Ministry of Trade, Industry and Energy (MOTIE), Republic of Korea (10050154, Establishment of Infrastructure for industrialization of Korean Useful Microbes, R0004073), and KFRI (Korea Food Research Institute, grant no: E0124200), and Hongik University Research Fund.

### Compliance with ethical standards

**Conflict of interest** Authors have no conflict of interest to declare.

### References

- H.E. Abaci, M.L. Shuler, *Integr. Biol. (Camb.)* **7**, 383–391 (2015)
- S. Alqahtani, L.A. Mohamed, A. Kaddoumi, *Expert Opin. Drug Metab. Toxicol.* **9**, 1241–1254 (2013)
- P. Artursson, K. Palm, K. Luthman, *Adv. Drug Deliv. Rev.* **46**, 27–43 (2001)
- B. Atac, I. Wagner, R. Horland, R. Lauster, U. Marx, A.G. Tonevitsky, R.P. Azar, G. Lindner, *Lab. Chip* **13**, 3555–3561 (2013)
- R. Baudoin, L. Griscom, J.M. Prot, C. Legallais, E. Leclerc, *Biochem. Eng. J.* **53**, 172–181 (2011)
- R.N. Bergman, *Journ. Annu. Diabetol. Hotel Dieu*, 127–138 (2007)
- Z. Brahmí, T. Katho, R. Hatsumata, A. Hiroi, N. Miyakawa, E. Yakou, K. Sugaya, J. Onose, N. Abe, *Biosci. Biotechnol. Biochem.* **76**, 1028–1031 (2012)
- T. Bricks, J. Hamon, M.J. Fleury, R. Jellali, F. Merlier, Y.E. Herpe, A. Seyer, J.M. Regimbeau, F. Bois, E. Leclerc, *Biopharm. Drug Dispos.* **36**, 275–293 (2015)
- V. Carriere, J. Chambaz, M. Rousset, *Toxicol. in Vitro* **15**, 373–378 (2001)
- M. Chi, B. Yi, S. Oh, D.J. Park, J.H. Sung, S. Park, *Biomed. Microdevices* **17**, 9966 (2015)
- A. Choe, S.K. Ha, I. Choi, N. Choi, J.H. Sung, *Biomed. Microdevices* **19**, 4 (2017)
- S. Choi, M. Nishikawa, A. Sakoda, Y. Sakai, *Toxicol. in Vitro* **18**, 393–402 (2004)
- C.M. Costello, R.M. Sorna, Y.L. Goh, I. Cengic, N.K. Jain, J.C. March, *Mol. Pharm.* **11**, 2030–2039 (2014)
- B. Davies, T. Morris, *Pharm. Res.* **10**, 1093–1095 (1993)
- M.T. Donato, A. Lahoz, J.V. Castell, M.J. Gomez-Lechon, *Curr. Drug Metab.* **9**, 1–11 (2008)
- M.B. Esch, G.J. Mahler, T. Stokol, M.L. Shuler, *Lab. Chip* **14**, 3081–3092 (2014)
- M.B. Esch, J.M. Prot, Y.I. Wang, P. Miller, J.R. Llamas-Vidales, B.A. Naughton, D.R. Applegate, M.L. Shuler, *Lab. Chip* **15**, 2269–2277 (2015)
- M. Gertz, A. Harrison, J.B. Houston, A. Galetin, *Drug Metab. Dispos.* **38**, 1147–1158 (2010)
- C.A. Gonzalez-Arias, A. Crespo-Sempere, S. Marin, V. Sanchis, A.J. Ramos, *Food Chem. Toxicol.* **86**, 245–252 (2015)
- R. Greek, A. Menache, *Int. J. Med. Sci.* **10**, 206–221 (2013)
- H.F. Helander, L. Fandriks, *Scand. J. Gastroenterol.* **49**, 681–689 (2014)
- D.D. Huh, *Ann. Am. Thorac Soc.* **12**(Suppl 1), S42–S44 (2015)
- K.I. Kaitin, *Clin. Pharmacol. Ther.* **87**, 356–361 (2010)
- H.J. Kim, D.E. Ingber, *Integr. Biol. (Camb.)* **5**, 1130–1140 (2013)
- H.J. Kim, D. Huh, G. Hamilton, D.E. Ingber, *Lab. Chip* **12**, 2165–2174 (2012)
- S.H. Kim, J.W. Lee, I. Choi, Y.C. Kim, J.B. Lee, J.H. Sung, *J. Nanosci. Nanotechnol.* **13**, 7220–7228 (2013)
- T. Kniazeva, A.A. Epshteyn, J.C. Hsiao, E.S. Kim, V.B. Kolachalam, J.L. Charest, J.T. Borenstein, *Lab. Chip* **12**, 1686–1695 (2012)
- Y.Y. Lau, Y.H. Chen, T.T. Liu, C. Li, X. Cui, R.E. White, K.C. Cheng, *Drug Metab. Dispos.* **32**, 937–942 (2004)
- S.A. Lee, Y. No da, E. Kang, J. Ju, D.S. Kim, S.H. Lee, *Lab. Chip* **13**, 3529–3537 (2013)
- J. Lee, B. Choi, Y. No da, G. Lee, S.R. Lee, H. Oh, S.H. Lee, *Integr. Biol. (Camb.)* **8**, 302–308 (2016)
- H. Lee, D.S. Kim, S.K. Ha, I. Choi, J.M. Lee, J.H. Sung, *Biotechnol. Bioeng.* **114**, 432–443 (2017)
- G.J. Mahler, M.B. Esch, R.P. Glahn, M.L. Shuler, *Biotechnol. Bioeng.* **104**, 193–205 (2009)
- I. Maschmeyer, A.K. Lorenz, K. Schimek, T. Hasenberg, A.P. Ramme, J. Hubner, M. Lindner, C. Drewel, S. Bauer, A. Thomas, N.S. Sambo, F. Sonntag, R. Lauster, U. Marx, *Lab Chip* **15**, 2688–2699 (2015)
- M.R. McGill, H. Jaeschke, *Pharm. Res.* **30**, 2174–2187 (2013)
- P.G. Miller, M.L. Shuler, *Biotechnol. Bioeng.* **113**, 2213–2227 (2016)
- C. Moraes, J.M. Labuz, B.M. Leung, M. Inoue, T.H. Chun, S. Takayama, *Integr. Biol. (Camb.)* **5**, 1149–1161 (2013)
- C. Oleaga, C. Bernabini, A.S. Smith, B. Srinivasan, M. Jackson, W. McLamb, V. Platt, R. Bridges, Y. Cai, N. Santhanam, B. Berry, S. Najjar, N. Akanda, X. Guo, C. Martin, G. Ekman, M.B. Esch, J. Langer, G. Ouedraogo, J. Cotovio, L. Breton, M.L. Shuler, J.J. Hickman, *Sci. Rep.* **6**, 20030 (2016)
- C.A. O'Neill, G. Monteleone, J.T. McLaughlin, R. Paus, *Bioessays* **38**, 1167–1176 (2016)
- D.A. Ouattara, S.H. Choi, Y. Sakai, A.R. Pery, C. Brochot, *Toxicol. Lett.* **205**, 310–319 (2011)
- J.M. Prot, L. Maciel, T. Bricks, F. Merlier, J. Cotton, P. Paullier, F.Y. Bois, E. Leclerc, *Biotechnol. Bioeng.* **111**, 2027–2040 (2014)
- R.B. Raffa, J.V. Pergolizzi Jr., R. Taylor Jr., J.F. Decker, J.T. Patrick, *Pain Pract.* **14**, 668–677 (2014)
- S.C. Ramaiahgari, M.W. den Braver, B. Herpers, V. Terpstra, J.N. Commandeur, B. van de Water, L.S. Price, *Arch. Toxicol.* **88**, 1083–1095 (2014)
- U. Sankar, *Scientist* **19**, 32–34 (2005)
- K.A. Scott, M. Ida, V.L. Peterson, J.A. Prendergill, G.M. Moloney, T. Izumo, K. Murphy, A. Murphy, R.P. Ross, C. Stanton, T.G. Dinan, J.F. Cryan, *Brain Behav. Immun.* (2017)
- J. Shemesh, I. Jalilian, A. Shi, G. Heng Yeoh, M.L. Knothe Tate, M. Ebrahimi Warkiani, *Lab Chip* **15**, 4114–4127 (2015)
- K.Y. Shim, D. Lee, J. Han, N.T. Nguyen, S. Park, J.H. Sung, *Biomed. Microdevices* **19**, 37 (2017)
- A. Sin, K.C. Chin, M.F. Jamil, Y. Kostov, G. Rao, M.L. Shuler, *Biotechnol. Prog.* **20**, 338–345 (2004)
- W.R. Stahl, *Science* **150**, 1039–1042 (1965)
- J. Strovel, S. Sittampalam, N.P. Coussens, M. Hughes, J. Inglese, A. Kurtz, A. Andalibi, L. Patton, C. Austin, M. Baltezor, M. Beckloff, M. Weingarten, S. Weir, *Early Drug Discovery and Development Guidelines: For Academic Researchers, Collaborators, and Start-up Companies (Assay Guidance Manual)*, G.S., 2004
- J.H. Sung, M.L. Shuler, *Ann. Biomed. Eng.* **40**, 1289–1300 (2012)
- J.H. Sung, C. Kam, M.L. Shuler, *Lab. Chip* **10**, 446–455 (2010)
- J.H. Sung, J. Yu, D. Luo, M.L. Shuler, J.C. March, *Lab. Chip* **11**, 389–392 (2011)
- J.H. Sung, M.B. Esch, J.M. Prot, C.J. Long, A. Smith, J.J. Hickman, M.L. Shuler, *Lab Chip* **13**, 1201–1212 (2013)
- J.H. Sung, B. Srinivasan, M.B. Esch, W.T. McLamb, C. Bernabini, M.L. Shuler, J.J. Hickman, *Exp. Biol. Med. (Maywood)* **239**, 1225–1239 (2014)
- L.M. Sweeney, M.L. Shuler, J.G. Babish, A. Ghanem, *Toxicol. in Vitro* **9**, 307–316 (1995)
- M. Takahashi, T. Washio, N. Suzuki, K. Igeta, S. Yamashita, *J. Pharm. Sci.* **98**, 4343–4353 (2009)

- N. Ucciferri, T. Sbrana, A. Ahluwalia, *Front Bioeng. Biotechnol.* **2**, 74 (2014)
- K. Viravaidya, A. Sin, M.L. Shuler, *Biotechnol. Prog.* **20**, 316–323 (2004)
- F. Vozzi, D. Mazzei, B. Vinci, G. Vozzi, T. Sbrana, L. Ricotti, N. Forggione, A. Ahluwalia, *Biotechnol. Bioeng.* **108**, 2129–2140 (2011)
- W.M. Westerink, W.G. Schoonen, *Toxicol. in Vitro* **21**, 1581–1591 (2007)
- J.P. Wikswo, E.L. Curtis, Z.E. Eagleton, B.C. Evans, A. Kole, L.H. Hofmeister, W.J. Matloff, *Lab. Chip* **13**, 3496–3511 (2013)
- S. Wilkening, F. Stahl, A. Bader, *Drug Metab. Dispos.* **31**, 1035–1042 (2003)
- J. Yu, S. Peng, D. Luo, J.C. March, *Biotechnol. Bioeng.* **109**, 2173–2178 (2012)
- T.J. Zurlinden, B. Reisfeld, *Eur. J. Drug Metab. Pharmacokinet.* **41**, 267–280 (2016). <https://doi.org/10.1007/s10544-017-0242-8>